Proceedings of the ASME 2010 3rd Joint US-European Fluids Engineering Summer Meeting and 8th International Conference on Nanochannels, Microchannels, and Minichannels
FEDSM-ICNMM2010
August 1-5, 2010, Montreal, Canada

FEDSM-ICNMM2010-31017

EXPERIMENTAL STUDY OF DYNAMIC INTERACTION BETWEEN A STEAM GENERATOR TUBE AND AN ANTI-VIBRATION BAR

V. Lalonde
BWC/AECL/NSERC Chair of Fluid-Structure Interaction,
Dep. of Mechanical Engineering, École Polytechnique de Montreal
Montreal, Quebec, Canada, H3C 3A7

A. Ross[1]
CREPEC
Dep. of Mechanical Engineering, École Polytechnique de Montreal
Montreal, Quebec, Canada, H3C 3A7

M. J. Pettigrew
BWC/AECL/NSERC Chair of Fluid-Structure Interaction,
Dep. of Mechanical Engineering, École Polytechnique de Montreal
Montreal, Quebec, Canada, H3C 3A7

I. Nowlan
CREPEC
Dep. of Mechanical Engineering, École Polytechnique de Montreal
Montreal, Quebec, Canada, H3C 3A7

ABSTRACT

A first experimental work was previously carried out to study the dynamic behavior of a tube simply supported at both ends in interaction with an anti-vibration bar at mid-span. This paper presents modifications to the previous setup with the aim of improving the accuracy of the results. A comparison of the dynamic behavior of the tube is made between both setups.

The objective of this experimental study is to characterize the vibration behavior of U-tubes found in steam generators of nuclear power plants. Indeed, two-phase cross-flow in the U-tubes section of steam generators can cause many problems related to vibration. In fact, flow-induced vibration of the U-tubes can cause impacts or rubbing of the tubes against their flat bar supports. Variation of the clearance between the AVB and the U-tubes may lead to ineffective supports. The resulting in-plane and out-of-plane motions of the tubes are causing fretting-wear and impact abrasion.

In this study, the clearance between the tube and the AVB, as well as the amplitude, form and frequency of the excitation force are controlled parameters. The first two modes of the tube are studied.

The modifications made to the setup lead to significant improvements in the results. The natural frequencies of both setups are compared to theoretical values. The difference between experimental and theoretical frequencies confirms that the new setup better represents the theoretical model of a simply supported tube. The damping of both setups is also compared to values found in literature. The results show that the new setup is more representative of realistic steam generator situations.

Compared to the first setup, the displacements of the new setup clearly indicate that the movement of the tube is mostly parallel to the flat bar and in the same direction as the excitation force. The whirling motion of the tube is prevented in the new setup. The accuracy of the contact force as a function of clearance was also improved. The use of more sensitive force sensors helped to reduce the noise level of the contact force.

Finally, the dynamic interaction between the tube and the AVB, defined by the fretting wear work-rate, presents a more consistent behavior. The maximum work-rate occurs when the tube is excited around the second mode for clearance between -0.10 and 0.00 mm. Such clearance between the tube and the AVB should then be avoided to minimize fretting damage.

[1] Corresponding Author

INTRODUCTION

The steam generators of a nuclear power plant are used to convert water into steam. In steam generators, thermal energy is transferred from a primary loop to a secondary loop. The primary loop contains high pressure water that circulates inside U-tubes while the secondary loop is a flow of water that circulates outside the tube bundles. Heat transfer takes place to convert water of the secondary loop into steam. Steam is then used to run turbines that provide electricity.

However, two-phase cross-flow on the secondary side induces vibration of steam generator U-tubes. A significant number of studies on vibration induced by cross-flow were conducted in the past few years [1-2]. To prevent large amplitude vibration, the tubes are supported by anti-vibration bars (AVB) in the U-bend region. The minimum clearance between U-tubes and AVB is set to allow tube thermal expansion and to reduce the risk of tube failures from fretting-wear. Unfortunately, larger clearances occur in some steam generators causing greater impacts and rubbing of the U-tubes against the AVB. Premature fretting damage often leads to tube failure, resulting into power plants shut-downs and costly repairs. Therefore, to avoid such damages it is necessary to understand the dynamic behavior of the tubes subjected to a two-phase cross-flow.

In two-phase cross-flow, the dynamic behavior usually depends on damping and vibration mechanisms. Several studies were conducted regarding two-phase cross-flow and their resulting mechanisms [3-10]. Damping mechanisms restrain the vibration response of the tubes by absorbing mechanical energy. On the other hand, the most important vibration mechanism is fluidelastic instability which occurs from the interaction between fluid-induced dynamic forces and tube motion. When the fluidelastic instability velocity is critical, the vibration response of the tubes increases drastically, causing large impacts and rubbing against the AVB. Random excitation forces due to turbulent flow and periodic wake shedding mechanisms can also have a contribution on the amplitude of excitation forces.

To predict steam generators U-tubes service life, fretting-wear work-rate is used [11]. Fretting wear depends on several factors such as the materials used for the tubes and AVBs, environmental conditions and the interaction behavior between the tubes and the AVBs. To predict the dynamic behavior of the tube interaction with the AVB and to estimate the fretting wear work-rate, many numerical models were developed [12-14]. These models are evolving as they are developed from experimental knowledge. These experimental studies are conducted to understand the vibration mechanisms encountered in steam generators [3].

An initial experimental study was previously carried out to characterize the dynamic behavior of a steam generator tube in interaction with an AVB [15]. The results obtained from this first setup were used to calculate the fretting wear work-rate which can be used to establish the service life of U-tubes. However, the low accuracy and the poor repeatability of these results were major problems encountered. To improve the accuracy, several modifications were made to the previous test rig and to the experimental procedure. This paper presents a comparison between the two setups to determine whether these changes contributed to upgrade the accuracy of the tests.

In the following sections, an overview of the design and fabrication of the two experimental setups is presented. To verify the improvement of the experimental setup, a vibration response analysis is done by comparing the two dynamic behaviors. Finally, the fretting wear work-rate is calculated from the new data and compared to the previous results.

EXPERIMENTAL SETUP

The objective of the experimental setup, shown on Fig. 1, is to study the dynamic behavior of a tube in interaction with a flat bar by duplicating a realistic steam generator tube/support configuration. To simplify the experimental model, a steam generator U-tube with the largest radius of curvature is represented by a simply supported straight tube. A fixed flat bar at mid-span is employed to reproduce a steam generator AVB. The tube (1) is provided with extension links at both ends, and is fixed to an I-beam mounting post (2) with bottom and top supports (3). The flat bar displacement assembly (4) is also screwed to the I-beam mounting post which is fixed to a structural concrete column of the building. Electromagnetic shakers (5) simulate the flow-induced vibration excitation forces and the test-rig is instrumented with laser displacement sensors, accelerometers and force sensors.

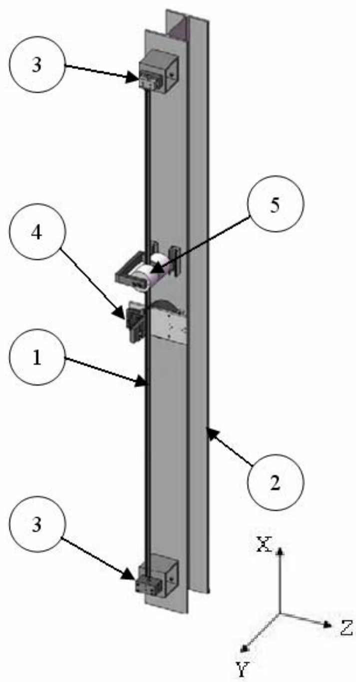

Figure 1-Experimental setup

The tube extension links and supports are shown in Fig. 2. The Inconel 690 tube is 2.5 mm long, has a 15.9 mm outer diameter and a 0.965 mm wall thickness. The stainless steel extension links at both ends of the tube are designed in the shape of a bone. They are built to allow bending and to support most of the flexion and the torsion. The cylindrical end of the bottom extension link (6) is inserted in the aluminum bottom support (7) and fixed with set screws (8) to prevent the rotation of the tube. The top extension link (9) is squeezed between two parts that include the top support (10) which are fixed with screws (11).

In the first experimental setup, the tube was provided with links with a thin round section of 5 mm diameter. The thin section of the links is the moving part that simulates a simple support. To make sure that most of the flexion and torsion is supported by the thinnest section of the link, the bottom link was reduced to a diameter of 3.81 mm.

Although the excitation force is in the Y direction, the tube in the first setup had an important displacement in the Z direction (axes are shown on Fig. 1). The tube displacement of both setups is presented in the next section. To uncouple the displacements in the Y and Z directions, the top link was modified. The link was changed to a square section instead of a round section. The side of the square is 3.33 mm. Consequently the tube is now preferentially flexible in the principal directions.

The bottom and top support positions of the new setup were also adjusted to ensure the verticality of the tube. They were aligned using a mass attached to a cable which was fixed to the top support. The position of the bottom support was then adjusted accordingly to ensure that the tube was fully vertical when fixed in it supports.

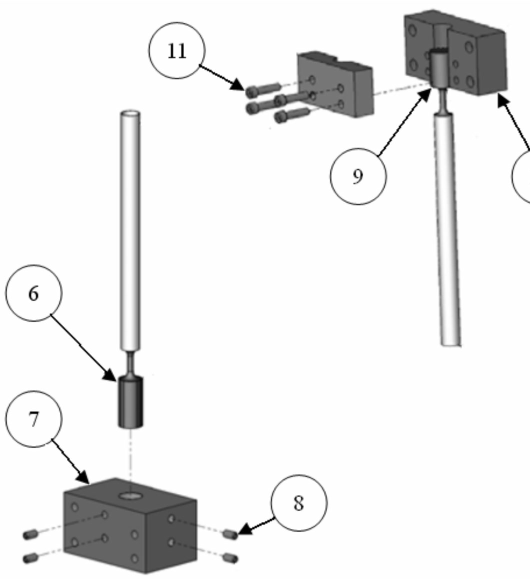

Figure 2-Extension links and supports assembly

The flat bar displacement assembly is shown in Fig. 3. The 410SS flat bar (12) (56 mm x 25.3 mm and 3.7 mm thick) is mounted on a 25 mm maximum displacement translation stage (13) and on a rotation stage (14) through a 90° bracket (15). The translation stage and the rotation stage have accuracies of 1 μm and 2 arc/sec, respectively. The flat bar displacement assembly allows to set different negative or positive clearances and different angles between the tube and the flat bar. A negative clearance between the tube and the flat bar corresponds to a preload (1mm = 0.545 N).

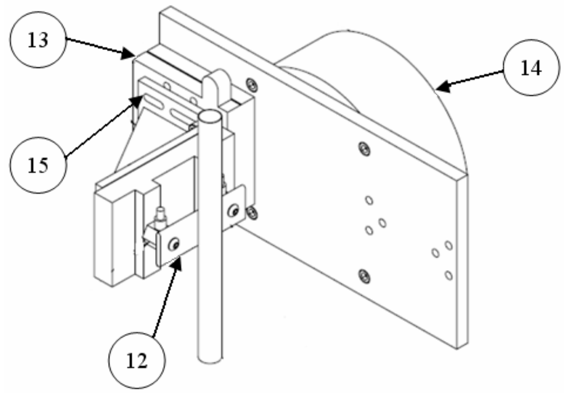

Figure 3-Flat bar displacement assembly

The electromagnetic shakers excite a ferromagnetic target located inside the tube with excitation forces parallel to the flat bar. The setup instrumentation is shown in Fig. 4. In the new setup, the shakers are placed at a higher position on the tube. Previously, the electromagnetic shakers were at 0.31 m from the center of the tube. They are now located at 0.88 m from the center in the new setup. This way, the required excitation force is reduced for the second mode since the electromagnetic shakers are farther away from the node at the middle of the tube (Fig. 6). However, the excitation force required to excite the fourth mode is increased. It was decided that studying the second mode was more important as explained in the next section.

In the first setup, two force sensors (16) of ±44.48 N measurement range and 112.4 mV/kN sensitivity were placed between the flat bar and the 90° bracket to measure contact forces between the tube and the bar. The forces measured with the first setup were much smaller than expected. To increase the accuracy of the results, new force sensors were installed. The test rig is now equipped with force sensors having a measurement range of ±9.79 N and a sensitivity of 494 mV/kN.

Two accelerometers (17) having a measurement range of 491 m/s^2 and a sensitivity of 10.19 $mV/(m/s^2)$ are positioned at 160 mm from the flat bar. The top accelerometer measures vibrations parallel to the flat bar (Y-axis) and the lower one measures vibrations perpendicular to the flat bar (Z-axis).

Finally, one pair of displacement laser sensors (18) having a measurement range of ±50 mm measures the tube displacement in directions Y and Z directly at the AVB level. Another pair is located 0.4 m below the electromagnetic shakers.

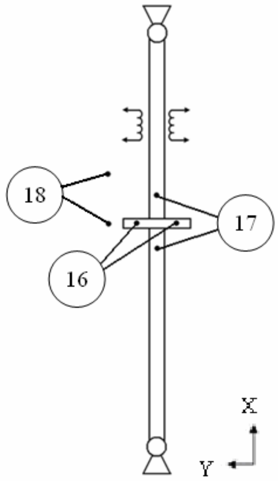

Figure 4-Setup instrumentation

In the first setup, the laser sensors were pointing directly on the curved surface of the tube. However, the curvature of the tube led to displacement reading errors because the laser was not always pointing at the center axis of the tube. To avoid such measurement error, rings with flat surfaces were installed on the tube as seen on Fig. 5. In the new setup, the laser sensors are pointing straight on the flat surfaces which are perpendicular to the laser beam.

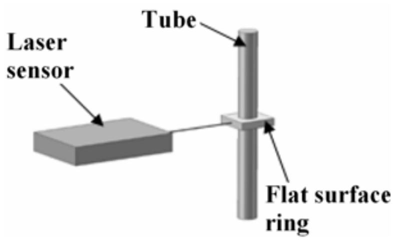

Figure 5- Modification of the laser sensors

PROCEDURES

Several modifications were made to the procedure from the first experimentation. In the previous procedure, the controlled parameters were the clearance and the orientation between the tube and the flat bar, the amplitude, the form and the frequency of the excitation force. The first experiment demonstrated that the orientation between the tube and the flat bar did not have a significant effect on the dynamic behavior. Thus, the orientation is no longer used as a controlled parameter in the new procedure.

All frequency spectra are obtained using real time frequency analyzer NVGate 4.22 and are plotted using Matlab 7.1. The input sampling is 51.2 ks/sec and the acquisition window is 100 sec.

The clearance between the tube and the flat bar is set manually with the translation stage. The zero position is determined visually. The clearances chosen for the first tests were between -0.35 mm and 0.25 mm in steps of 0.05 mm. The results obtained from the first experimental setup showed trends in the tube acceleration, force and displacement response. Some of the clearances were then eliminated from the experimental procedure while still maintaining sufficient accuracy in the results. For excitation forces around odd modes, a focus on positive clearances is more important than on negative clearances. On the other hand, for excitation force around even modes, negative clearances are more important in this study.

The excitation force was applied around the first four natural frequencies to excite the mode shapes seen on Fig. 6. The results clearly illustrate that the behavior was the same for all odd modes. A different pattern was also shown for all even modes. For this reason, only excitation forces around the first and the second modes are studied in the new procedure.

The previous tests also supported the conclusion that the use of a white noise within a 10 Hz bandwidth was acceptable to estimate the turbulence vibration observed in a steam generator [15]. This form of excitation force is used in the new procedure.

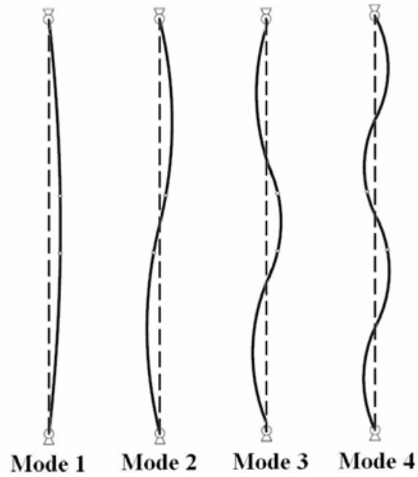

Figure 6- Mode shapes

The amplitude of excitation force used in the tests is calculated and averaged using the root mean square value (RMS). To determine the RMS force amplitude, a calibration is done on a short tube excited by the electromagnetic shakers. In the first procedure, two force sensors were used to measure the RMS force as a function of the electromagnetic power which was measured with a multi-meter. The readings of voltage and amperage were used to calculate the electromagnetic shaker power which was a linear function of the RMS force. Since there were great fluctuations of voltage and amperage during the acquisition, the voltage signal is now obtained as an input in the acquisition device. This way, the voltage signal is directly seen on the frequency spectrum. The RMS force is then plotted as a function of the voltage for excitation forces around each mode. During an acquisition, the voltage frequency spectrum is used to determine the related RMS force.

Since modifications were made to the extension links and because the electromagnetic shakers were placed at a higher position on the tube, the tube mechanical impedance decreased. To obtain the same displacements in the Y direction as in the previous experiments, the required RMS force applied on the tube is then reduced. Table 1 shows a comparison between the RMS forces used in both experiments.

Table 1- Correlation between excitation force amplitudes

		First setup	New setup
Mode 1	**F_{RMS} min (N)**	0.035	0.007
	F_{RMS} max (N)	0.076	0.013
Mode 2	**F_{RMS} min (N)**	0.058	0.012
	F_{RMS} max (N)	0.076	0.017

VIBRATION RESPONSE ANALYSIS

Natural frequencies

An impact test was conducted to obtain the experimental natural frequencies of the tube. The acceleration cross-spectrum, that represents the resultant acceleration in the two axes, is then used to identify the natural frequencies of the tube at the acceleration peaks. A first test was done on the tube without the flat bar. To verify that the natural frequencies remained the same when the flat bar was in contact with the tube, a second impact test was conducted with a zero clearance. Figure 7 shows the acceleration cross-spectra from the two impact tests for the new setup.

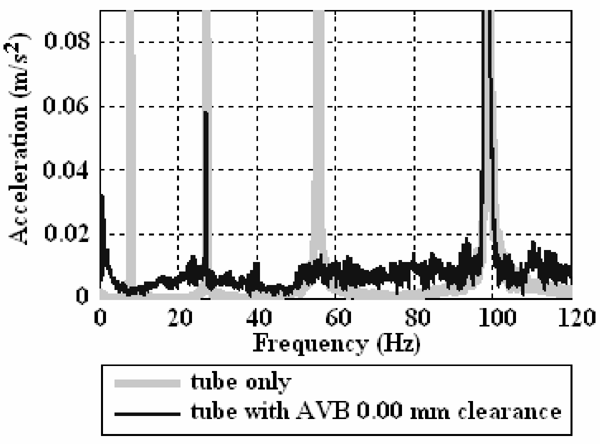

Figure 7-Acceleration cross-spectrum for an impact test on the tube

As seen in Fig. 7, the presence of the AVB has no effect on the natural frequencies of even modes, which have a node at the flat bar location. However, the odd modes are eliminated by the presence of the bar at their antinodes.

In Table 2, the first five experimental natural frequencies of each setup are compared to the theoretical values of a simply supported tube to determine which setup is closer to the theory.

Table 2- Comparison of natural frequencies

	Experimental		Theoretical	Relative errors	
Mode	**First setup**	**New setup**	**Simply supported**	**First setup**	**New setup**
	Hz	**Hz**	**Hz**	**%**	**%**
1	8.1	7.3	6.6	22.7	9.8
2	28.0	26.5	26.5	5.7	0.0
3	59.5	55.0	59.6	0.2	7.7
4	99.8	98.0	105.9	5.8	7.5
5	158.6	158.8	165.5	4.2	4.1

The relative errors with respect to theoretical natural frequencies, shown in Table 2, confirm that the new setup is a better representation of the theoretical model. The changes made to the extension links of the tube contributed to the decrease in the natural frequencies. The relative errors show that there was considerable improvement on the first two natural frequencies, which belong to the modes studied in this paper. Unfortunately, the natural frequencies of modes 3 and 5 are more distant from the theoretical values compared to the first setup. However, these differences are less significant than the improvements on the first two modes.

Damping

The mechanical energy dissipated by structural damping can be deduced from the width of the natural frequency peaks. The damping is estimated by the half-power bandwidth method. A sine sweep excitation force around the first mode is used and the average damping ratio is calculated from the average of nine acceleration cross-spectra. The expression used to evaluate the damping is:

$$\xi = \frac{f_2 - f_1}{2 f_n} = \frac{\Delta f}{2 f_n} \quad \text{for } A = \frac{A_n}{\sqrt{2}} \qquad (1)$$

ξ is the damping ratio

A_n is the acceleration peak amplitude

f_n is the natural frequency at A_n.

f_1, f_2 are the frequencies at A

The peak width Δf is estimated from an interpolation of the experimental data. This interpolation is in fact a quadratic function plotted from the data points of the peak.

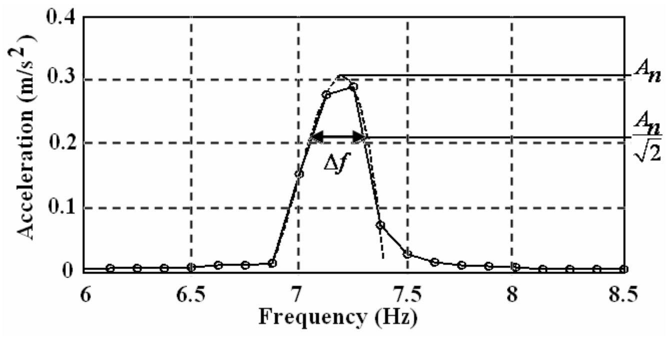

Figure 8- Acceleration cross-spectrum-Sinusoidal sweep-Mode 1

The measured damping of each setup without flat bar is compared to damping values in the literature for a simply supported tube to determine which setup is more representative of realistic steam generator situations.

Table 3- Damping comparison

Experimental damping		Damping in literature
First setup	**New setup**	**Steam generator**
0.9	0.018	0.015

The damping values shown in Table 3, confirm that the new setup is more representative of a U-tube in a steam generator. However, the experimental values are somewhat higher than expected. This behavior can be explained by additional damping in the extension links of the tube.

Displacement Lissajous figures

Laser sensor pairs at the electromagnetic shaker and at the AVB measure the tube displacements in the drag and the lift directions. In Fig. 9 and Fig. 10, a comparison of the displacement for both setups is presented for three different clearances, i.e.: -0.25 mm, 0.00 mm, and 0.25 mm, and for excitation forces around the first and the second mode.

When the tube vibrates around the first mode, the measured displacement for a positive clearance is greater at the AVB level than at the electromagnetic shaker level, as expected from the mode shape in Fig. 6.

The first experimental setup reveals a whirling motion of the tube for a positive clearance of 0.25 mm (Fig. 9a). No impact or contact can be detected from the figure (there is no abrupt change in the direction of the motion). On the other hand, the new setup shows that the movement of the tube is mostly in the Y direction, parallel to the flat bar and in the same direction as the excitation force (Fig. 9d). The modification made to the top extension link contributed to the alignment of the displacement in the Y direction. The whirling motion of the tube, probably caused by dissymmetry, is avoided since the tube is preferentially flexible in two directions.

Compared to the first setup, the new setup clearly shows the prevailing sliding motion of the tube against the flat bar for zero clearance (Fig. 9b and e). The tube motion is restrained in the Z direction as it slides and impacts on the AVB. The Y displacement is smaller for the zero clearance than for the larger clearance of 0.25 mm.

In both setups, there is no significant motion of the tube for a negative clearance of -0.25 mm (Fig. 9c and f). In this case, the AVB acts as a support.

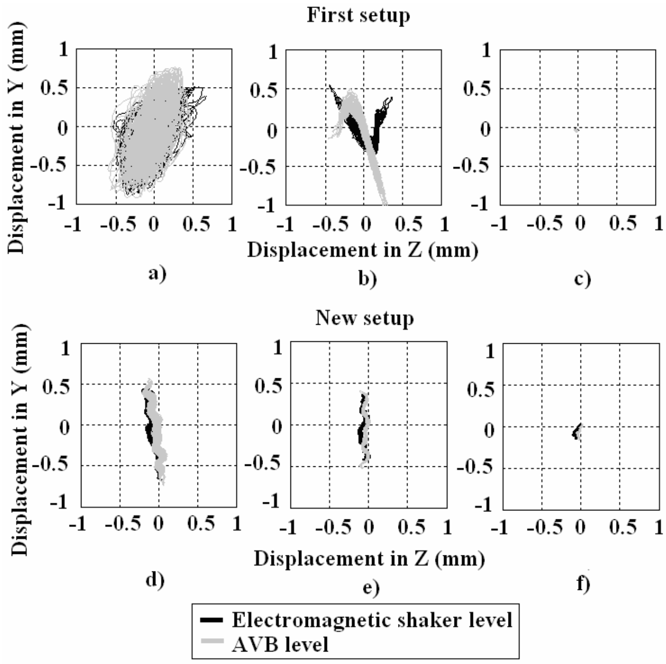

Figure 9- Comparison of Lissajous figures - Mode 1
a) 0.25 mm clearance, first setup b) 0.00 mm clearance, first setup
c) -0.25 mm clearance, first setup
d) 0.25 mm clearance, new setup e) 0.00 mm clearance, new setup
f) -0.25 mm clearance, new setup

For excitation forces around the second mode, the mode shape indicates that there is a node at the flat bar (Fig. 6). There should then be no considerable motion of the tube at the AVB.

However, the first experimental setup shows an important motion of the tube at the AVB for a clearance of 0.25 mm (Fig. 10a) and 0.00 mm (Fig. 10b). Compared to the first setup, the displacement observed at the AVB in the new setup is small for all three clearances (Fig. 10d, e and f). At the electromagnetic shaker, the displacement is mainly parallel to the flat bar, and at approximately the same amplitude for all clearances.

In fact, the clearance should not have an important effect on the tube displacement because the flat bar is directly located at a node of the tube. Restraining the node should not change the tube response. This behavior is clearly observed with the new setup.

On the Lissajous figures of the new setup, the curves are slightly tilted with respect to the line Z=0 (Fig. 10d, e and f), although less than for the first setup. This behavior can be explained by possible misalignment of the flat surface on which the laser sensor is pointing. If the laser sensor is not totally parallel to the flat surface, such error will then be observed on the displacement. The misalignment of electromagnetic shakers can also be responsible for this behavior.

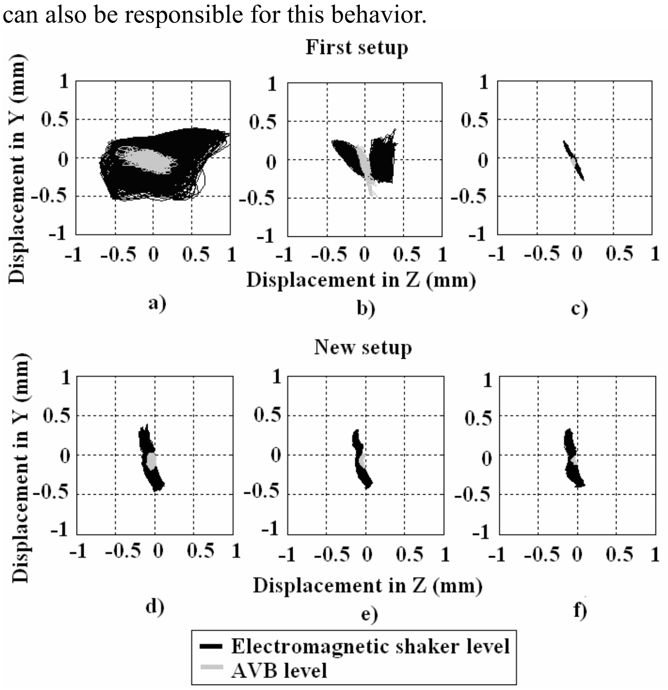

Figure 10- Comparison of Lissajous figures - Mode 2
a) 0.25 mm clearance, first setup b) 0.00 mm clearance, first setup
c) -0.25 mm clearance, first setup
d) 0.25 mm clearance, new setup e) 0.00 mm clearance, new setup
f) -0.25 mm clearance, new setup

Contact force spectra

The two force sensors supporting the flat bar are used to obtain the contact force spectra. Figure 11 compares the contact force spectra as a function of clearance for both setups.

Harmonic frequencies can be observed from the force cross spectra of the first mode in each setup (Fig. 11a and c). For clearances higher than 0.00 mm, there is a harmonic every 7.25 Hz, which corresponds to the first natural frequency. These harmonics are caused by impacts between the tube and the flat bar. The contact force amplitude increases between 0.00 mm and 0.10 mm and decreases for larger clearances. The major difference between the previous and the new setup is observed for negative clearances where the fifth and sixth harmonics are clearly noticeable in contact forces of the new setup. More studies are needed to explain this observation.

For excitation forces around the second mode, the contact forces are obviously maximum at the second natural frequency when there is a preload between the tube and the flat bar (Fig. 11b and d). There is no significant contact force between the tube and the flat bar for positive clearances. Significant harmonics can also be observed at higher frequencies for negative clearances in the new setup. More experimental data is required to explain this observation.

The variation of contact force amplitude at the natural frequency as a function of clearance can also be obtained from the contact force spectrum. Figure 12 compares the behavior between the two setups for excitation forces around modes 1 and 2 for two different excitation force levels.

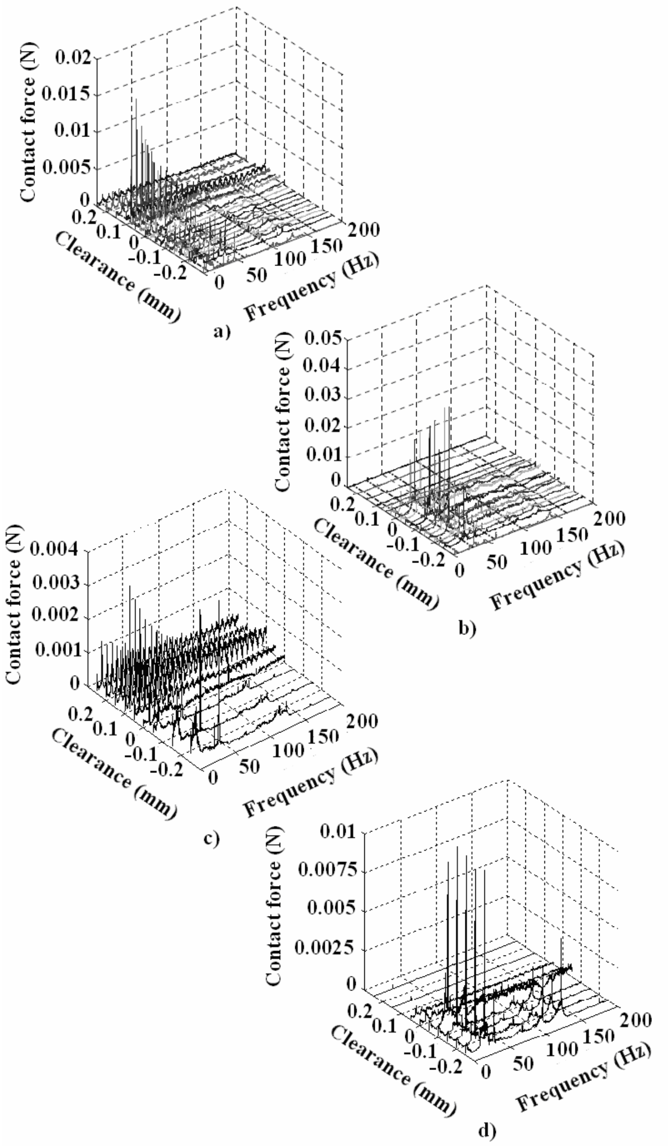

Figure 11- Comparison of force cross-spectra
a) Mode 1, first setup b) Mode 2, first setup c) Mode 1, new setup
d) Mode 2, new setup

As seen on the graphs for excitation force around the first mode (Fig. 12a and c), the force as a function of clearance follows the same trend in both setups. The force is small when the flat bar stops the motion of the tube with negative clearance. The force becomes larger as the clearance increases and reaches a maximum value at 0.10 mm. For clearances higher than 0.10 mm, the contact force decreases.

When the tube is excited at the second mode, the mode shape of the tube has a node in the middle. The contact force amplitude for excitation force around the second mode is negligible for positive clearance (Fig. 12b and d). The results obtained with the new setup clearly reveal that the contact force is constant for different preloads between the tube and the flat bar. According to observations, the contact forces obtained from the new setup are more appropriate and more reliable than the previous.

For both setups, the contact force amplitudes are higher at the second mode than at the first mode for clearances corresponding to a preload. In fact, the tube displacement at mid-span is the same in both modes for negative clearances (see Fig. 9f and Fig. 10f), but the tube vibrates at a higher frequency in the second mode. Therefore, the acceleration of the tube at the AVB is necessarily higher in the second mode, and the impact force is thus higher as well.

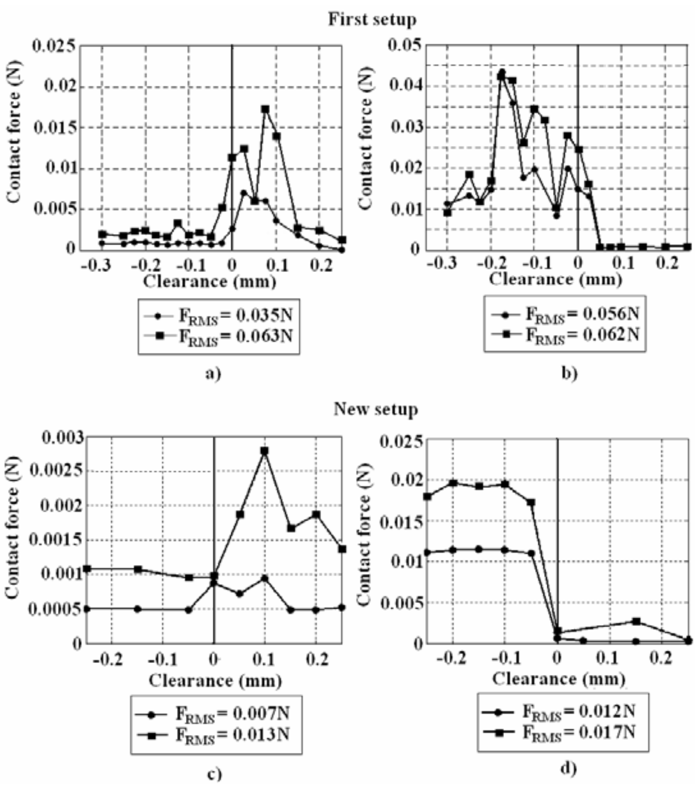

Figure 12- Comparison of force at natural frequency
a) Mode 1, first setup b) Mode 2, first setup c) Mode 1, new setup d) Mode 2, new setup

FRETTING-WEAR ANALYSIS

The volume rate of removed material is used to quantify tube fretting wear. The volume-rate and the normal work-rate are related by the following equation:

$$\dot{V} = K\dot{W}_N \qquad (2)$$

$\dot{V}$ is the volume rate of removed material

$\dot{W}_N$ is the normal work-rate

The wear coefficient K is obtained from experiments and depends on the material combination of the tube and the AVB and on specific operation conditions.

The work-rate can be calculated with the following expression:

$$\dot{W}_N = \int_{T_1}^{T_2} F_N ds \qquad (3)$$

F_N is the normal contact force between the tube and the AVB

s is the displacement of the tube parallel to the AVB

$T_2 - T_1$ is the time interval.

To ensure adequate tube service life, the work-rate should not exceed 1mW [16].

The time signal of the contact force and the time signal of the Y displacement at the AVB are used to calculate the work-rate. However, the signals of each sensor must be corrected to reduce noise. To correct the force signal, the mean noise level is used. Time data below the noise level threshold is eliminated from the calculation and the signal is reset to zero as shown on Fig. 13. For the first setup, the total noise level of the combined force sensors is set to -0.111 N. In the new setup, the total noise level is set to -0.066 N.

To correct the displacement time signal of the laser sensors, a lower bound and an upper bound are obtained from the noise time signal. In the first experiment, the bounds are respectively -80.65 µm and 24.60 µm. For the new setup, the measured bound are set to -75.55 µm and -37.63 µm. The signal located between those bounds is eliminated from the work-rate calculations.

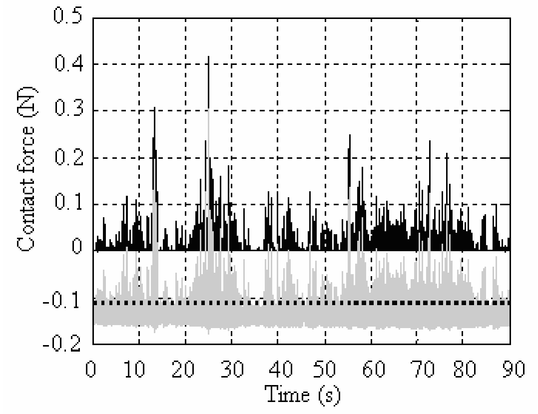

Figure 13- Noise correction of the contact force time signal: measurement (grey); noise threshold (dotted); corrected signal (full black)

Figure 14 shows the work-rate as a function of clearance for excitation force around the first and the second mode. The work-rate values are averaged over five measurements.

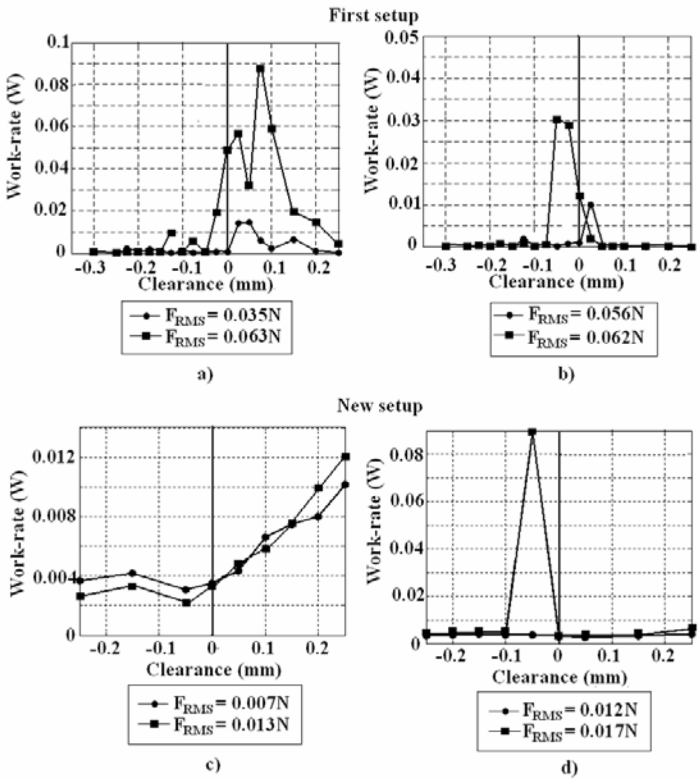

Figure 14- Comparison of work-rate as a function of clearance a) Mode 1, first setup b) Mode 2, first setup c) Mode 1, new setup d) Mode 2, new setup

For excitation forces around the first mode (Fig. 14a and b), the work-rate obtained from the first setup increases with clearance and reaches a maximum value for a clearance of 0.075 mm. With the new setup, the results show that work-rate is steady for different preloads between the tube and the flat bar and increases between -0.05 mm and 0.25 mm. The excitation force amplitude does not seem to have a significant effect on work-rate since both curves for F_{RMS} = 0.007 N and F_{RMS} = 0.013 N are similar. For both setups, the work-rate is greater than 1 mW but the overall work-rate of the new setup is about 10 times smaller than the first setup since the contact force is also smaller for the new setup (the displacement amplitude is similar for both setups).

For excitation forces around the second mode (Fig. 14b and d), the work-rate of both setups increases considerably around -0.10 mm to 0.00 mm clearance for high excitation forces. There appears to be a discontinuity in Fig. 14d, where a large spike can be seen, only because there is a single data point between -0.10 mm and 0.00 mm. More data points would be desirable and would likely lead to similar results as for the first setup. For low excitation forces, the clearance does not seem to have a significant effect on the work-rate which remains small. However, the work-rate for excitation force around the second mode is higher than 1mW for all clearances.

CONCLUSION AND RECOMMENDATION

The accuracy of the measurements is the major difference between the two setups. Accuracies of the displacement, contact force and clearance are important factors to determine whether or not a support is effective.

The accuracy of the displacement measurements is clearly improved by the addition of flat surface rings to the tube. The Lissajous figures of the new setup indicate that the movement of the tube is mostly in the Y direction, parallel to the flat bar and in the same direction as the excitation force. The whirling motion of the tube is prevented in the new setup. To improve the results, the perpendicularity between the laser sensors and the flat surfaces must be maintained.

The noise level of the contact force was reduced with the more sensitive force sensors. Harmonic frequencies can be observed from the force cross-spectrum of the first mode in each setup. These harmonics are caused by impacts between the tube and the flat bar. For excitation force around the second mode, the contact forces are obviously maximum at the second natural frequency for different preloads. No significant contact force between the tube and the flat bar was measured for positive clearances. However, the contact forces are so small that most of it is lost in noise for both setups. To improve the accuracy, force sensors with an even greater sensitivity would be desirable.

In spite of measurement problems, the trends of work-rate against clearance are clear for each mode. The overall uncertainties were greatly improved by the modifications to the setup. The work-rate values were also averaged over five acquisitions to improve accuracy.

It was shown that the maximum work-rate occurs for clearances between -0.10 and 0.00 mm. Large clearances can also contribute to increase the work-rate since the contact forces are then larger. From the results obtained in this paper, a negative clearance corresponding to a preload is desirable to avoid fretting-wear damage.

ACKNOWLEDGMENTS

The authors gratefully acknowledge the financial support of BWC, AECL and NSERC.

REFERENCES

[1] Price, S. J., & Paidoussis, M. P. (1983). Fluidelastic Instability of an Infinite Double Row of Circular Cylinders Subject to a Uniform Cross-Flow. *Journal of Vibration, Acoustics, Stress, and Reliability in Design*, 105, 59-66

[2] Price, S. J., Mark, B., & Paidoussis, M. P. (1986). An Experimental Stability Analysis of a Single Flexible Cylinder Positioned in an Array of Rigid Cylinders and Subject to Cross-Flow. *Journal of Pressure Vessel Technology*, 108, 62-71.

[3] Janzen, V. P., Hagberg, E. G., Pettigrew, M. J., & Taylor, C. E. (2005). Fluidelastic Instability and Work-Rate Measurements of Steam-Generator U-Tubes in Air-Water Cross-Flow. *Journal of Pressure Vessel Technology*, 127, 84-91.

[4] Pettigrew, M. J., & Taylor, C. E. (1994). Two-Phase Flow-Induced Vibration: An Overview. *Journal of Pressure Vessel Technology*, 116, 233-253.

[5] Pettigrew, M. J., Taylor, C. E., & Kim, B. S. (1989). Vibration of Tube Bundles in Two-Phase Cross-Flow: Part 1-Hydrodynamic Mass and Damping. *Journal of Pressure Vessel Technology*, 111, 466-477.

[6] Pettigrew, M. J., Tromp, J. H., Taylor, C. E., & Kim, B. S. (1989). Vibration of Tube Bundles in Two-Phase Cross-Flow: Part 2-Fluid-Elastic Instability. *Journal of Pressure Vessel Technology*, 111, 478-487.

[7] Taylor, C. E., Currie, I. G., Pettigrew, M. J., & Kim, B. S. (1989). Vibration of Tube Bundles in Two-Phase Cross-Flow: Part 3-Turbulence-Induced Excitation. *Journal of Pressure Vessel Technology*, 111, 488-500.

[8] Pettigrew, M. J., Tromp, J. H., & Mastorakos, J. (1985). Vibration of Tube Bundles Subjected to Two-Phase Cross-Flow. *Journal of Pressure Vessel Technology*, 107, 335-343.

[9] Pettigrew, M. J., & Taylor, C. E. (2003). Vibration Analysis of Shell-and-Tube Heat Exchangers: An Overview-Part 1: Flow, Damping, Fluidelastic Instability. *Journal of Fluid and Structures*, 18, 469-483.

[10] Pettigrew, M. J., & Taylor, C. E. (2003). Vibration Analysis of Shell-and-Tube Heat Exchangers: An Overview-Part 2: Vibration Response, Fretting-Wear, Guidelines. *Journal of Fluid and Structures*, 18, 485-500.

[11] P. L. Ko. (1979). Experimental Studies of Tube Frettings in Steam Generators and Heat Exchangers, *ASME Journal of Pressure Vessel Technology,* 101, 125-134.

[12] Hassan, M., & Hayder, M. (2008). Modeling of Fluidelastic Vibrations of Heat Exchanger Tubes with Loose Supports. *Nuclear Engineering and Design*, 238, 2507-2520.

[13] Fisher, N. J., Olesen, M. J., Rogers, R. J., & Ko, P. L. (1989). Simulation of Tube-to-Support Dynamic Interaction in Heat Exchange Equipment. *Journal of Pressure Vessel Technology*, 111, 378-384.

[14] Hassan, M. A., & Rogers, R. J. (2005). Friction Modelling of Preloaded Tube Contact Dynamics. *Nuclear Engineering and Design*, 235, 2349-2357.

[15] Nowlan, I. (2008). *Etude expérimentale du comportement vibratoire d'un tube de générateur de vapeur en interaction avec une barre plate*, Masters Thesis (École Polytechnique de Montréal), 136p.

[16] Yetisir, M., & Fisher N. J. (1997). Prediction of Pressure Tube Fretting-Wear Damage Due to Fuel Vibration, *Nuclear Engineering and Design,* 176, 261-271.